AADE-22-FTCE-058

Improved Understanding of Gas Influx Behaviors During Riser Gas Events: A Data Assimilation Approach

Chen Wei, Louisiana State University; and Yuanhang Chen, Louisiana State University

ABSTRACT

Riser gas events during offshore drilling operations are hazardous and challenging to control. Such events are difficult to accurately model due to the lack of knowledge of both liquid and gas phase inflow rate at the bottom of the riser, and gas influx distributions along the wellbore, leading to large uncertainties in the model prediction results. An Extended Kalman Filter (EKF) is used in this study as a data assimilation method for real-time estimation of gas and liquid inflow rate and improved accuracy of the transient two-phase flow models.

A set of full-scale experiments were carried out to simulate riser gas events in a Water-Based Mud (WBM) system, where a 5,000-ft deep onshore experimental wellbore was analogized as an offshore well. With pressure transducers installed at multiple depths of the well, the upper portion of the wellbore simulates the marine riser, while the lower portion represents the wellbore beneath the subsea blowout preventer (SSBOP). Real-time measurement data, including surface and downhole pressure, pump rate, and the liquid outflow rate, are used to estimate both phase inflow rates at the SSBOP level using the EKF. An online calibrated Drift Flux Model (DFM) based on data assimilation is used to estimate the distributed flow parameters, including the profiles of gas void fractions in the riser. The gas flow rate measured by a Daniel flowmeter and the Distributed Acoustic Sensing (DAS) data were used to validate the estimation results. Satisfying agreement between the estimation and the measurements was observed.

The benefits of this work are seen by maximizing the use of measurement data of different types, especially for wells equipped with Managed Pressure Drilling (MPD) systems, realizing more accurate modeling of gas migration behaviors in a riser. The inclusions of online model calibration with coefficients adaptively tuned help to further improve the accuracy of the existing physics-based models and help the design of riser gas management strategies.

INTRODUCTION

The ability to perform accurate estimation of the downhole influx rate and the distribution of formation gas kicks is of great importance for simulating a riser gas event, particularly when the gas kick is to be circulated out through the riser using Managed Pressure Drilling (MPD) systems. Gas kick simulation based on single and static input data are prone to accumulate errors and leads to instability in the prediction accuracy of the results. Thus, in managed pressure drilling operations, real-time model-based gas kick simulations are of great importance to provide immediate and accurate control of the well pressure management installations (Gu et al. 2020). Due to great uncertainties that exist in modeling wellbore two-phase flow during gas kick events, previous researchers have established several methods to improve the estimation accuracy. In the works of Kaasa et al. (2012) and Lorentzen et al. (2003), a Lyapunov-based adaptive observer is designed to estimate uncertain friction and density in the annulus and the bottomhole pressure in a well during drilling. According to Gravdal et al. (2010), an ensemble Kalman filter methodology was used to tune the uncertain parameters of a well-flow model in an underbalanced drilling operation. In the work of Lohne et al. (2008), friction calibration factors in the drillstring and annulus are tuned with an unscented Kalman Filter technique using topside and bottom-hole pressure measurements.

The Kalman filter was originally developed for linear models. An early approach for treating nonlinear models is the Extended Kalman filter (EKF). This has been used as the standard technique for performing recursive nonlinear estimation. However, the EKF is based on linearization and has shortcomings for strongly nonlinear models. Recently, an alternative filter with performance superior to that of the EKF has been developed, namely the unscented Kalman filter (UKF), first proposed by Julier et al. (1995) and Julier and Uhlmann (1996, 1997) and further developed by Van der Merwe and Wan (2001), Van der Merwe et al. (2000a and 2000b), and Wan and van der Merwe (2000 and 2001). The ensemble Kalman filter (EnKF) is based on a Monte-Carlo approach, using an ensemble of model representations to build up the necessary statistics. In Lorentzen et al. (2001), continuous updating of a well-flow model for underbalanced drilling was considered. Simple closure relations that depend on uncertain parameters were used

in the flow-model formulation. These uncertain parameters were tuned from time to time to minimize the differences between model predictions and measured data.

The primary indicators of a gas kick are increases in pit volume or flow rate from the well and a flowing well with pumps off (Hargreaves et al. 2001; Schubert et al. 2006; Luan et al. 2013; Romo and Plaisance 2015). It is useful to offer some considerations on these indicators and some newer proposed detection methods to place the present contribution in the proper context. A point to stress is the crucial importance of timely kick detection because delays add to the difficulty of well control and can lead to blowouts (Carlsen et al. 2013; Yang et al. 2019; Li et al. 2020). This point is so vital that some authors consider this aspect one of the key performance indicators of kick-detection methods (Fraser et al., 2014). If formation fluid flows into the wellbore, more drilling fluid will be ejected from the well than is pumped down through the drillstring, and this will cause an increase in the mud-pit volume (Anfinsen and Rommetveit 1992; Swanson et al. 1997). Although this is true in principle, in practice, pit gain can be caused by factors other than kicks. For example, a variety of transient effects such as the transport of cuttings, variations in the retention capacity of some components, pressure-loss variations, mud compressibility, and thermal expansion can cause pit gains (Cayeux and Daireaux 2017). Furthermore, the method has a somewhat low sensitivity because of the large volume of pits and is relatively slow because of the time needed for mud circulation (Luan et al., 2013). It is also the case, as will be shown later, that the rate of pit gain remains low and therefore difficult to detect until it is too late to take adequate measures.

Currently, there has been a limited number of applications on Kalman Filter techniques in Managed Pressure Drilling and well control scenarios. Meanwhile, the estimation of parameters with Kalman Filters has been focusing on single dimension parameters. In this study, considering the great nonlinearities between the controlling parameters and wellbore flow dynamics, the Extended Kalman Filter (EKF) as one of the improved Kalman Filters is implied.

1. Wellbore Two-phase Flow Models

1.1 Model Assumptions

The Drift Flux Model was first proposed by Zuber and Findlay (1965) as a correlation for predicting steady-state void-fraction profiles and later used in transient representations of one-dimensional multiphase flow dynamics in oil and gas well-drilling and production. The DFM gives simplification to the transient two-fluid model by replacing the separate momentum equations of both the liquid and gaseous phases with a mixture momentum equation and the slip law as a static closure relation (Wang et al., 2014; Aarsnes, 2016c). The derivation of the control equations of the DFM is based on the following assumptions (Nwaka et al. 2020).

a. Liquid-gas two-phase flow in the wellbore is considered a one-dimensional flow.
b. Gas and liquid phases have the same pressure and temperature at the same time and spatial location.
c. The effects of solids (e.g., cuttings) in the wellbore multiphase flow are ignored.
d. The two-phase flow in the wellbore is considered an isothermal process. The fluid temperature profile is known along the wellbore and remains unchanged during the simulated processes.
e. The mass transfer between liquid and gaseous phases is ignored.

1.2 Flow Equations

The Drift Flux Model was a simplification of the transient two-fluid model obtained by replacing the dynamic momentum equation of each phase with a mixture momentum equation and a static relation typically called a slip law. The governing equations of DFM are two mass conservation equations and one momentum conservation equation. The classical drift flux model formulation for one-dimensional two-phase flow is described by the following equations.

$$\frac{\partial(\alpha_l\rho_l)}{\partial t}+\frac{\partial(\alpha_l\rho_l v_l)}{\partial h}=\Gamma_l \tag{1}$$

$$\frac{\partial(\alpha_g\rho_g)}{\partial t}+\frac{\partial(\alpha_g\rho_g v_g)}{\partial h}=\Gamma_g \tag{2}$$

$$\frac{\partial(\alpha_l\rho_l v_l+\alpha_g\rho_g v_g)}{\partial t}+\frac{\partial(\alpha_g\rho_g v_g^2+\alpha_l\rho_l v_l^2+p)}{\partial h}=-S_p \tag{3}$$

Where α_g, α_l are gas, liquid void fractions; ρ_g, ρ_l are gas, liquid densities; v_g, v_l are gas, liquid absolute phase velocities, p is the pressure of both gas and liquid phase; $S_p$is the pressure source term; and t, h represents time and depth along the wellbore.

In this study, the gas influx migration behavior in WBM is studied exclusively and mass transfer between the gas and liquid phase is not considered. Therefore, $\Gamma_l=\Gamma_g=0$.
The source term S_p is defined as:

$$S_p=\frac{dp_f}{dh}+\frac{dp_g}{dh} \tag{4}$$

Where the gradational pressure gradient along the wellbore

$$\frac{dp_g}{dh}=g\left(\alpha_l\rho_l+\alpha_g\rho_g\right)cos\theta \tag{5}$$

represents the gravity source where g is the gravitational constant and θ is the wellbore inclination from the vertical. The viscous forces and forces between the mud and the wall are considered through the frictional pressure term $\mathrm{d}p_f/\mathrm{d}h$ given by

$$\frac{dp_f}{dh} = \frac{2f\rho_m v_m |v_m|}{D_o - D_i} \quad (6)$$

Where f is the friction factor that is a function of the two-phase Reynolds number.

1.3 Closure Equations

Because there are seven unknown variables (α_g, α_l , ρ_g , ρ_l , v_g , v_l , p) and just three flow equations, additional equations are needed to close the system of differential equations. The closure laws are normally required in terms of density models for each phase, a model for frictional pressure loss, and a slip relation since we consider the relative movement of the gas phase with respect to the liquid phase.
By far, the most important aspect of the model is the hydrodynamic/slip closure law, which is commonly expressed in the following general form:

$$v_g - v_l = \phi(m_g, m_l, v_g) \quad (7)$$

Where ϕ is the slip relation function.
The formulation of this law has a large effect on the flux Jacobian of the DFM and hence on the construction of a linearized numerical solver. In this study, a special case of this slip law presented by Zuber and Findlay (1965) is used as one of the closure equations as given by:

$$v_g = C_0 v_m + v_{gr} \quad (8)$$

The liquid density is assumed to have the form:

$$\rho_l = \rho_{l,0} + \frac{p - p_{l,0}}{a_l^2} \quad (9)$$

Where, $a_l = 1000\ \mathrm{m/s}$ is the liquid phase sonic velocity (Wang et al., 2014; Evje and Kjell, 2002) and $\rho_{l,0}$, $p_{l,0}$ are the liquid density and pressure at reference conditions. The gas-phase density is described as (Wei and Chen, 2021):

$$\rho_g = \frac{p}{a_g^2} \quad (10)$$

Where, $a_g = 316\ \mathrm{m/s}$ is the gas phase sonic velocity (Evje and Kjell, 2002). The gas and liquid phase volume fractions are related by:

$$\alpha_l + \alpha_g = 1 \quad (11)$$

1.4 Numerical Methods

Roe Scheme is one type of FDS scheme using the Roe approximate Riemann solver to solve the control equations. Roe solver, devised by Phil Roe (1981), is an approximate Riemann solver based on the Godunov scheme and involves finding an estimate for the intercell numerical flux or Godunov flux $f_{i+1/2}(\boldsymbol{w})$ at the interface between two computational cells $\boldsymbol{w_i}$ and $\boldsymbol{w_{i+1}}$. On some discretized space-time computational domain. The Roe method consists of finding a matrix $\widetilde{\boldsymbol{R}}(\boldsymbol{w_i}, \boldsymbol{w_{i+1}})$ that is assumed constant between two cells. The Riemann problem can then be solved as a truly linear hyperbolic system at each cell interface.

According to the study of Phil Roe (1981), instead of using the exact Riemann solver, the existence of a fast, approximate solver to the Reimann problem or Euler equations is found to be more generally useful. This numerical scheme is observed to be very accurate in modeling two-phase shock tube problems. Meanwhile, it can be used to reduce the number of iterations needed to obtain any more exact solutions which may be required. Fjelde et. al. (2002) and Munkejord. (2006) implemented Roe's FDS Scheme in the solution of the drift flux model.

The Roe Scheme was chosen in this study to enable the implementation of an Extended Kalman Filter with the drift flux model, where the state transition function that applied to the previous state to acquire the current system state can be explicitly expressed using the Jacobian Matrix.

1.5 The Jacobian Matrix

The model that expressed as Eqn. (1), (2), (3) can be written in the following vector form:

$$\frac{\partial \boldsymbol{q}}{\partial t} + \frac{\partial \boldsymbol{f}(\boldsymbol{q})}{\partial x} = \boldsymbol{s}(\boldsymbol{q}) \quad (12)$$

Where $\boldsymbol{q}$ is the vector of conserved variables, $\boldsymbol{f}$ is the vector of fluxes, and $\boldsymbol{s}(\boldsymbol{q})$ is the vector of sources. They are given by:

$$q = \begin{bmatrix} \alpha_l\rho_l \\ \alpha_g\rho_g \\ \alpha_l\rho_l v_l + \alpha_g\rho_g v_g \end{bmatrix} = \begin{bmatrix} m_g \\ m_l \\ I_g + I_l \end{bmatrix} \quad (13)$$

$$\boldsymbol{f}(\boldsymbol{q}) = \begin{bmatrix} \alpha_l\rho_l \\ \alpha_g\rho_g v_g \\ \alpha_l\rho_l v_l^2 + \alpha_g\rho_g v_g^2 + p \end{bmatrix} = \begin{bmatrix} I_g \\ I_l \\ I_g v_g + I_l v_l \end{bmatrix} \quad (14)$$

and

$$\boldsymbol{s}(\boldsymbol{q}) = \begin{bmatrix} 0 \\ 0 \\ -F_w \end{bmatrix} \quad (15)$$

Since the momentum equation is for the two-phase mixture, a supplementary hydrodynamic closure law, commonly denoted as the slip relation, is required to determine the velocity of each phase. In addition, thermodynamic closure laws are needed for each phase to relate the phasic density to the mixture pressure. The drift-flux model can be written in conservation form, and it has been shown to be hyperbolic for a reasonable range of input parameters (Romate, 1998). However, even for simple closure relations, the Jacobian of the model becomes rather complicated.

An alternative formulation of the system (Eqn. (1), (2), (3)) is the quasilinear form

$$\frac{\partial \boldsymbol{q}}{\partial t} + \boldsymbol{A}(\boldsymbol{q})\frac{\partial \boldsymbol{q}}{\partial x} = \boldsymbol{s}(\boldsymbol{q}) \tag{16}$$

where the flux Jacobian $A(q)$ is defined as

$$\boldsymbol{A} \equiv \frac{\partial \boldsymbol{f}}{\partial \boldsymbol{q}} = \left[\frac{\partial f_i}{\partial q_i}\right] \tag{17}$$

Derive the expression for $\boldsymbol{A}$, gives the Jacobian matrix:

$$A(q) = \frac{1}{\varrho}\begin{bmatrix} m_g m_l \mu_g + \zeta m_g m_l & m_g m_l \mu_l - m_g \mu_l & m_g \\ -(m_g m_l \mu_g + \zeta m_g m_l) & m_g \mu_l - m_g m_l \mu_l & \zeta m_l \\ a_{31} & a_{32} & 2(m_g \mu_g + \zeta m_l \mu_l) \end{bmatrix} \tag{18}$$

Where,

$$a_{31} = \kappa \varrho \rho_l + 2m_g m_l(\mu_g - \mu_l) + (\zeta m_l - m_g)\mu_g^2 - 2\zeta m_l u_g u_l$$

And

$$a_{32} = \kappa \varrho \rho_l + 2m_g m_l(\mu_g - \mu_l) - (\zeta m_l - m_g)\mu_g^2 - 2\zeta m_l u_g u_l$$

2. Data Assimilation Methods

2.1 Extended Kalman Filter

The implemented Drift Flux Model based on Equations (1) - (3), solved explicitly based on the Jacobian Matrix, can conceptually be represented as:

$$X_k = f(X_{k-1}, \theta) + q_k \tag{19}$$

$$y_k = h(X_k) + r_k \tag{20}$$

Where $q_k \sim N(0, Q_{k-1})$ is the zero-mean Gaussian process noise and model error, and $r_k \sim N(0, R_k)$ is the zero-mean Gaussian measurement noise.

2.2 The Joint State Vector

The Kalman Filter based on a linearized model was developed to estimate both state and parameter of the system to estimate both state parameters of the system, usually known as augmented Kalman Filter. Dual and joint KF techniques are two common approaches for the estimation of parameters and state variables simultaneously. The dual FK uses another Kalman Filter for parameter estimation so that two filters run sequentially in every time step, the state estimator updates with new measurements, and then the current estimate of the state is used in the parameter estimator. The joint KF augments the original state variables with parameters, and a single filter is used to estimate the augmented state vector. In this study, a Joint EKF is used. The augmented state vector at time instant k is written as:

$$\begin{bmatrix} X_k \\ \theta_k \end{bmatrix} = \begin{bmatrix} f(X_{k-1}, \theta_{k-1}) - q_k \\ \theta_{k-1} \end{bmatrix} = f^a(X_{k-1}, \theta_{k-1}) + q_k^a \tag{21}$$

For the implementation of an Extended Kalman Filter with the drift flux models, we need the Jacobian of the explicit formulation of the system equation. A first-order Taylor series expansion is applied, written as $F(\bar{X}_{k-1}, \bar{X}_k) = 0$.

$$F(X_{k+1}, X_k)X_{k+1} + F(X_{k+1}, X_k)X_k = 0 \tag{22}$$

Where $F(\bar{X}_{k-1}, \bar{X}_k)$ if F with respect to a X_k. Hence, for the system Jacobian, we get

$$J = -F_{X_{k+1}}^{-1}(X_{k+1}, X_k)F_{X_k}(X_{k+1}, X_k) \tag{23}$$

Where the partial derivatives are evaluated at the trajectory. We recognize $F_{X_{k+1}}$ to the Jacobian, previously discussed, the inverse of which is known to exist.

2.3 System Uncertainty Quantification

a. Model Error

The model error consists of both an initial error and an accumulating error term, with covariance matrixes Q_0 and Q_k respectively. In this context, we assume that the model error for the well flow variables is accounted for by the uncertainty in the model parameters. This is done because the well flow parameters have a notable impact on the flow behavior. The friction parameters influence the pressure gradient, while the slip parameters directly affect the flow velocities and flow rates. In addition, it is difficult to produce good estimates of the uncertainty of the discretized flow variables and the correlations which inevitably exist between them. We assume Q_k to be time-independent, and it can be written as

$$\{Q\}_{ij} = \begin{cases} 0 \ , if\ i \neq j, i\ or\ j \leq M \\ \in, if\ i = j \leq M \\ \left(\sigma_i^Q\right)^2, if\ i = j > M \\ \sigma_i^Q \sigma_j^Q \rho_{ij}^Q, otherwise \end{cases} \tag{24}$$

where M is the number of variables in v, and $\in$ is a small positive number that ensures that Q is positive definite. We note that $\rho_{i,j}^Q$ must be chosen to preserve positive definiteness. The matrix Q_0 is expressed in the same manner. The values ρ_{ij}^Q represent the correlation coefficients for the model errors related to the parameters. It is difficult to obtain accurate values for these correlations, and several values have been tried in the process leading to the results shown here. If no correlation between the parameters was assumed, we experienced cases where the parameters drifted towards unphysical values. This is since parameters can counteract, and several compositions can produce the same result. Based on this, we have chosen a common correlation $\rho_{ij}^Q = \rho_{ij}^{Q_o} = 0.90$ between all the

parameters. (The value for these correlation coefficients is also based on experience resulting from the examples in Lorentzen et al., 2001).

b. Measurement Error

The covariance matrix R_k must be specified to apply the ensemble Kalman filter. In this context, we assume that measurement errors are uncorrelated. As done in Cohn (1997), the measurement error can be split into a term related to the measurement device and one term which is state-dependent due to a discretized numerical model (representativeness error).

The surface backpressure, bottom hole pressure, and liquid outflow rates are used as measured variables. The pressure was measured from five pressure sensors installed at different depths within the wellbore. We assume that flow rates and pump pressure are evaluated at the cell boundaries and that representativeness error can be neglected for these values. The uncertainty is, therefore, only related to the measurement gauge. A value of 5% is adopted for the rate measurements, and 1.5 % is used for the pressure.

Calculation of other pressure values is, however, subject to uncertainty in the numerical method, as this utilizes average pressure values. An interpolation is needed to gain the pressure values which correspond to the measured values. There is also uncertainty related to the position of the measurement gauge. We assume that the pressure gauge is in the middle of a grid box and that the grid box is filled with 50% gas. If we neglect fluid velocities and pressure contribution due to the presence of gas, we can obtain the uncertainty in the pressure readings.

3. Simulation Results and Discussion

3.1 Full-scale Experimental Data

A set of full-scale experiments was conducted at the experimental well facility at Louisiana State University (LSU) to fully understand the gas migration behaviors during a riser gas event. Riser gas events were simulated by injecting gas (Nitrogen) from the bottom of the experimental wellbore that is filled with water. The flow parameters, including pressure, temperature, and flow rates, were measured at multiple depths in the wellbore. And a Fiber Optic Sensing (FOS) system (including Distributed Acoustic Sensing (DAS) and Distributed Temperature Sensing (DTS)) was installed for the high-resolution monitoring of the two-phase flow dynamics in the annulus. The schematic of the experimental wellbore is shown in **Fig.1**, which is a vertical onshore wellbore with a total depth of 5,024 ft, a casing size of 9-5/8 inches, and a simulated drilling pipe diameter of 2-7/8 inches.

In real-world offshore drilling operations, the measurement of pressure at the SSBOP level is possible to acquire using underwater sensors, for example, the BOP pressure probes that are designed to measure the fluid pressure at the bottom of the riser usually installed above the blind rams. The pressure readings of the fluid in the riser are available in real-time through electrical lines when the annular BOP is not closed.

In an onshore wellbore, when taking a gas kick downhole, the inflow rate of liquid (drilling fluid) at the bottom of the wellbore is considered to know or can be easily estimated based on the pump rate. However, for an offshore well, the inflow rate of both liquid and gaseous phases into the drilling riser at a depth of the Blowout Preventer (BOP) is unknown and difficult to measure directly. As a matter of fact, the inflow rate of liquid at a certain moment can be significantly higher or lower than the pump rate, depending on the different two-phase flow dynamics in the wellbore beneath the mud line. Therefore, to define the inflow condition of a marine riser, both phase inflow rates should be considered as unknown parameters. In this section, the time series inflow rate of the liquid phase (q_l) and gaseous phase (q_g) were estimated simultaneously based on real-time measurement data.

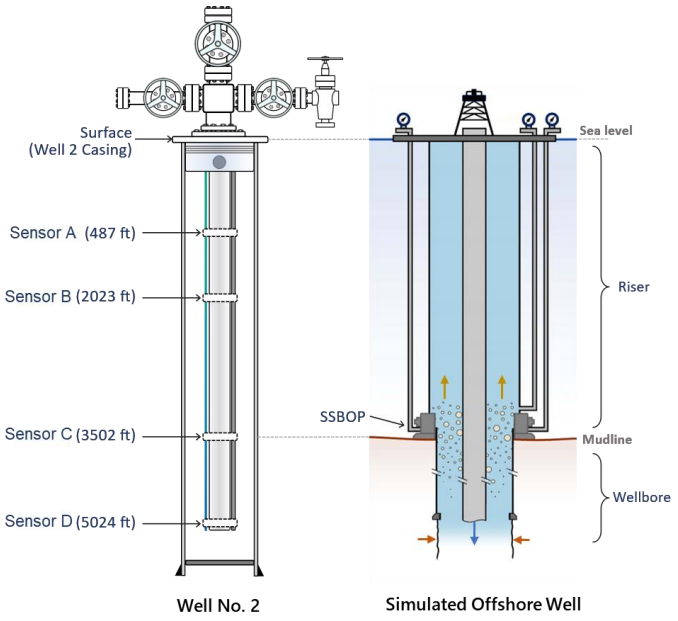

Fig. 1. The schematics of the full-scale experimental wellbore and the analogy to a drilling riser

To replicate such uncertainty in the inflow conditions in a real riser gas event, the experimental wellbore was analogized as an offshore well. As shown in **Fig. 1**, five pressure transducers are installed at different depths of the experimental wellbore (0 ft, 487 ft, 2023 ft, 3502 ft, and 5024 ft). The upper wellbore section from the surface to a depth of 3,502 ft is analogized as the drilling riser, while the wellbore section from 3502 ft to 5024 ft represents the wellbore below the SSBOP. The pressure measurement at "Sensor C" (**Fig. 1**) will represent the SSBOP pressure in the following sections. Therefore, the goal of this simulation is to estimate the flow rate of liquid and gas at a depth of Sensor C based on the measurement data available at

the surface and downhole.

3.2 Model Validation

To validate the accuracy of the proposed transient two-phase flow models as well as the data assimilation methods, simulation results using only the DFM and a DFM combined with data assimilation method based on single-depth or multiple-depth measurements are compared with true measurement data. Two processes, including a gas injection process and a gas circulation process, are included in the simulation. From approximately 750 seconds to 1800 seconds, a 30 bbl (at downhole conditions) gas kick was injected to the bottom of the experimental well through the chemical injection line that runs directly to the same depth of the tubing (simulated drillpipe). After the end of the injection, the drill pump was started and maintained at a 100 gal/min rate until the gas kick was completely removed from the well.

In the full-scale experiment, a Daniel flowmeter was installed on the Nitrogen injection line on the surface. The injection rate of gas was measured at the surface in standard cubic feet per min (SCF/min). This data was used for the validation of the estimated gas injection rate based on the data assimilation method. However, since the influx rate is directly estimated under downhole conditions, the flow rate measured from the Daniel flowmeter was converted from surface conditions to downhole conditions using a PVT sub-model. In this section, the gas inflow boundary conditions are defined at the bottom of the wellbore, and the liquid inflow is considered known as the pump rate that is directly measured.

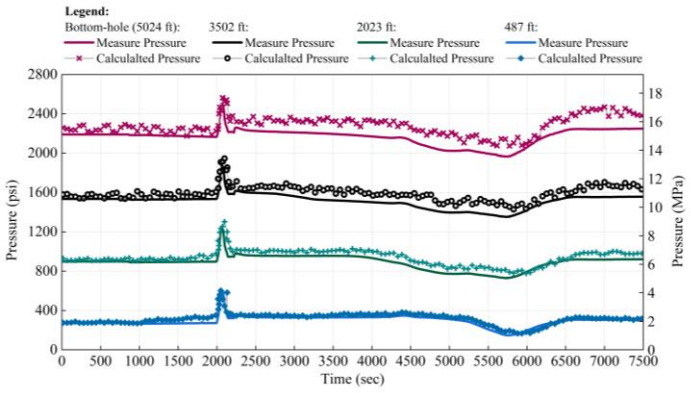

Fig 2. Comparison of Measured Pressure and Estimated Pressure at Different Depth (DFM Only)

The presented DFM was used to estimate the mixture pressure and both-phase flowrate distributions. A 10 percent synthetic noise is added to both the model input data and the prediction results. The estimation results of pressure at the depths of downhole pressure transducers using only the DFM are compared with the experimental measurements, as shown in **Fig. 2**.

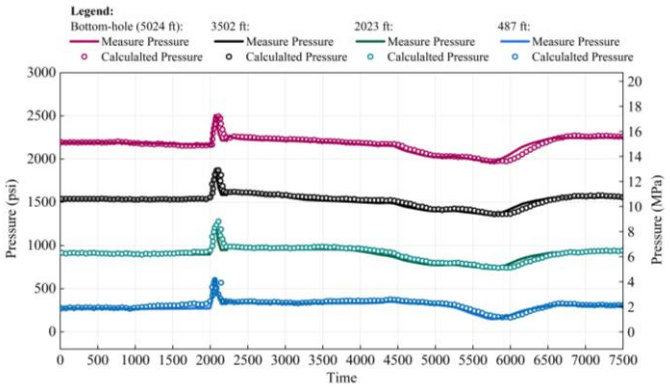

Fig 3. Comparison of Measured Pressure and Estimated Pressure at Different Depth (DFM with Data Assimilation)

Fig 3. presents the estimation results of pressure at different depths using the DFM combined with the Extended Kalman Filter. The same levels of synthetic noises were added to both the model input data and the prediction results. The multi-depth pressure measurement with artificial noises was fed into the Kalman Filter as real-time observations. From **Fig. 3**, the estimation results of pressure at different depths show higher accuracy when the EKF is implemented. The noise signals included in the measurement data and prediction results are well filtered using the EKF. According to **Fig. 2**, the estimation error/noise is larger at the depths close to the surface. This is because the input data is given at the inlet boundary at the bottom, and the error will accumulate when the boundary effect propagates upward along the annulus.

3.3 Gas and Liquid Inflow Rate Estimation

Observation Data Input for the EKF

The change of pressure at the SSBOP level (3,502 ft), the mud outflow rate measured at the surface, and the surface backpressure over time were used as observations data for the Extended Kalman Filter to update the model predictions and to estimate the unknown downhole influx rates.

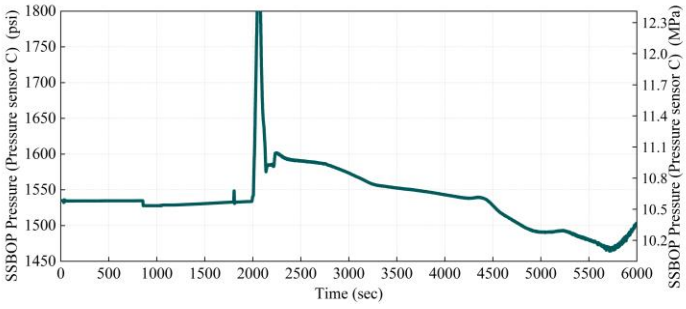

Fig. 4. The Time-Series SSBOP Pressure (Pressure Sensor C) Measurement Data

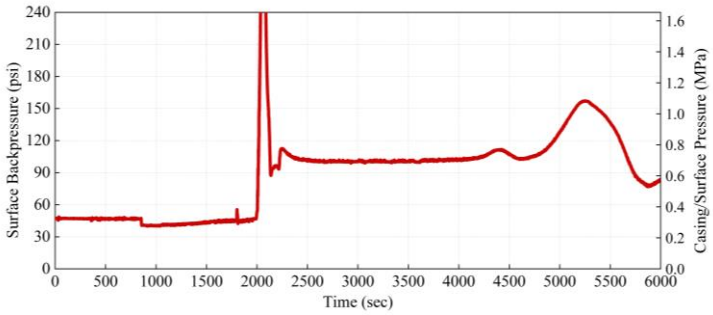

Fig. 5. The Time-Series Surface Backpressure Measurement Data

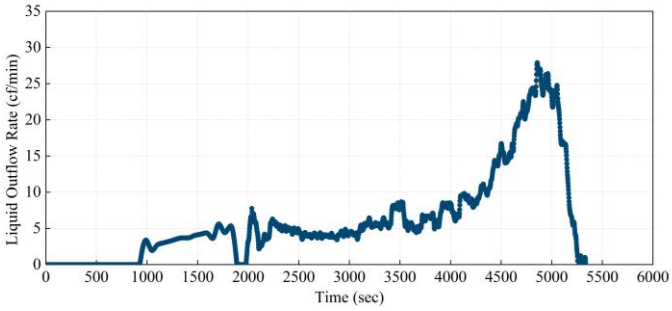

Fig. 6. The Time-Series Liquid Outflow Rate Measurement Data

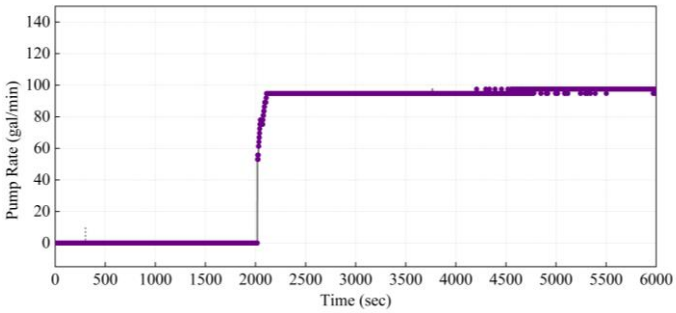

Fig. 7. The Time-Series Pump Rate Measurement Data

Fig. 4 to 7 demonstrate the time-series measure data of the SSBOP pressure, surface backpressure, liquid outflow rate, and pump rate. As aforementioned, the gas injection process lasted from approximately 750 seconds to 1,800 seconds, during which the pump was not running. After the end of injection, the drill pump started and maintained a 100 gal/min rate to circulate the gas kick out of the wellbore. At approximately 5,800 seconds after the experiment started, the gas influxes were seen at the surface, and a peak value of surface pressure and outflow rate, as well as a minimum bottom-hole pressure, were observed.

Although the pump rate does not directly represent the liquid inflow rate at the SSBOP level, practices have proven that the inclusion of the pump rate as an observation input helps with improving the converging performance of the Extended Kalman Filter in the reverse estimation of the unknown flow rates.

For the input data and boundary conditions used in the Drift Flux Model, the measured casing pressure at the surface was considered as the outlet boundary condition. Since both the gas and liquid inflow rate are designed to be estimated based on real-time measurement data, a single-phase liquid flow with the same flow rate of the pump output is used as an initial condition assumption to represent a normal drilling scenario at the very beginning.

For the outlet boundary conditions, mass flow rates and convective fluxes are obtained using a simple extrapolation method referring to the adjacent cells, as proposed by Wang et al. (2010). The measured time-series surface backpressure is used as the outlet pressure boundary conditions, as shown in **Fig. 5**.

Estimation Results of Both Phase Inflow Rate

Based on the above proposed methods, the inflow rate of both liquid and gas at a depth of Sensor C (SSBOP) was estimated simultaneously. The estimation results are shown in **Fig. 8** and **Fig. 9**.

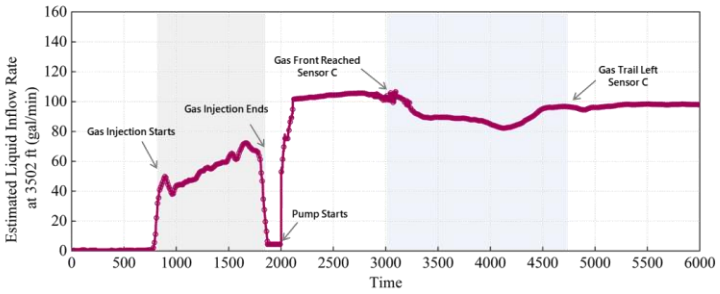

Fig. 8. Estimated Liquid Inflow Rate at the Depth of Pressure Sensor C (3502 ft)

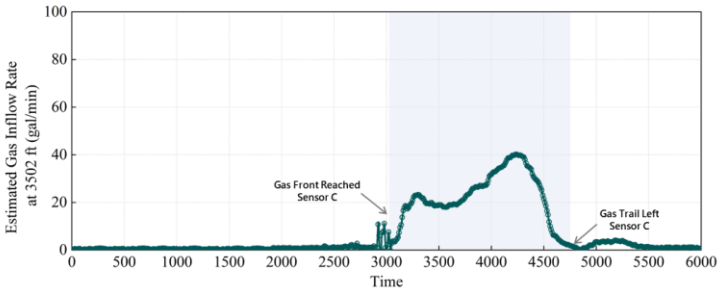

Fig. 9. Estimated Gas Inflow Rate at the Depth of Pressure Sensor C (3502 ft)

During the gas injection process (from 750 seconds to 1800 seconds), a liquid flow rate of approximately 40-70 gal/min was observed at the depth of pressure sensor C. This is due to the displacement of water by the nitrogen injected from the bottom.

This rate matches well with the liquid outflow measured at the surface, as shown in **Fig. 6**. Since the gas influx stayed at a deeper location during this period, the gas flow rate maintained zero. When gas injection was completed, and the pump was not yet started, the liquid flow rate quickly reduced to 7.33 gal/min. This value is non-zero because of the expansion of the injected gas.

After circulation started at approximately 2000 seconds, the estimated liquid flow rate raised up to 106.3 gal/min and gradually increased over time. This phenomenon was also explained by the expansion of gas in the annulus while migrating upward. At 3,050 seconds after the experiment started, the gas flow rate started to increase at the depth of 3,502 ft, representing the front of the gas influx has reached the location of pressure sensor C. Meanwhile, the liquid flow rate started to decrease due to the higher void fraction in the gas section. At 4,810 seconds, the gas inflow rate reduced to near zero, and the liquid flow rate stabilized at approximately 100 gal/min. This represents the tail of the gas section has passed the depth of pressure Sensor C. As an analogy, this represented a gas influx that has completely entered the drilling riser.

Here we shall keep in mind that no direct information of any actual gas and the liquid flow rate was fed into the Drift Flux Model, and all the estimation results were deduced from the indirect measurement data. In general, the above estimation has a good agreement with the actual operation during the experiment and our overall understanding of the gas migration behaviors in the wellbore. Yet, to fully validate the performance of the proposed method in estimating both phase inflow rates, further comparison of the estimation with measured data will be given in the following subsections.

Estimation of Gas Void Fraction Distribution

Take the estimation results of both phase inflow rate as shown in **Fig. 8** and **Fig. 9** as the input data, and the measured surface backpressure as the outlet pressure boundary condition, a profile of gas void fraction in the riser can be calculated, as well as the evolution of gas distribution versus time (as shown in **Fig. 12**). The upward migration behavior and the expansion of the formation gas influx were observed as represented by the void fractions. The top boundary of the gas influx reaches the surface approximately 5,890 seconds after the simulation begins. The maximum gas void fraction at the wellhead during this process is approximately 0.69 when influx reaches the surface. The timing of gas reaching the surface shows a good agreement with the real observation during the experiments.

However, to further validate this estimation, we are lacking the direct measurement of void fraction in the wellbore. As a matter of fact, the measuring of void fractions along a drilling well remains challenging nowadays. In this section, the model estimation results based on an online calibrated Drift Flux Model were used for comparison. Instead of only simulating the multiphase flow dynamics in the upper wellbore (0 ft to 3,502 ft), the gas migration behavior from the bottom of the well (5,024 ft) was calculated. The gas injection rate measured by the Daniel Flowmeter (as shown in **Fig. 10**) and the actual pump rate (as shown in **Fig. 7**) were used as model inputs.

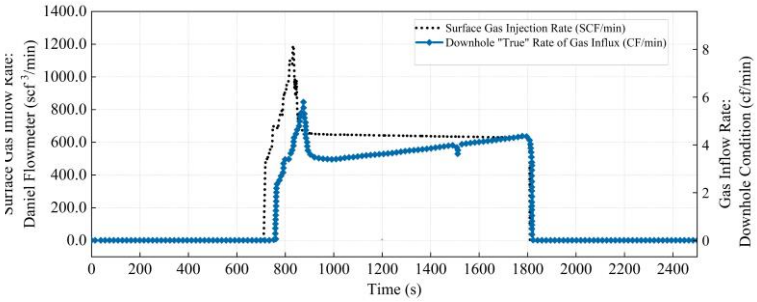

Fig 10. The Measurement of Gas Injection Rate Based on the Daniel Flowmeter

In the standard drift-flux approach, the closure of the system is achieved by specifying a slip model between the phases. The slip law as aforementioned can be expressed by the equation:

$$v_g = C_{0,d}\left(\alpha_g v_g + \alpha_l v_l\right) + C_{1,d} = C_{0,d} v_{mix} + C_{1,d} \tag{25}$$

In addition, it is necessary to provide an appropriate model for the frictional pressure loss term in the momentum equation. A frequently used expression for this term is:

$$K = C_f \frac{2f}{D} \rho_{mix} v_{mix}^2 \tag{26}$$

In equations (25) and (26), the empirical coefficients $C_{0,d}$, $C_{0,d}$ and C_f are defined as slip coefficients and friction coefficients and tuned during the data assimilation procedure. Using the Joint EKF as presented in section 2., these three coefficients were updated in real-time to obtain a high degree of simulation accuracy. The tuning of the values of the coefficients over time is displayed in **Fig. 11**.

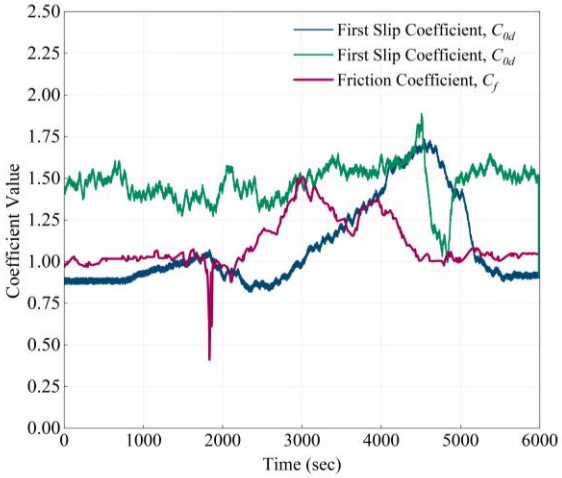

Fig. 11: Real-time Tuning of Empirical Model Coefficients

Taking real measurement data as input, and with the help of online model calibration, we now obtained an estimation of the void fraction profiles with relatively higher confidence. Although such estimation will not be able obtained in real drilling operations, we can use it in the section for the validation of the estimation results based on the proposed method. As shown in **Fig. 12**, overall good agreement can be observed by comparing the estimated void fraction profiles calculated based on measured influx rate and estimated influx rate using the data assimilation method. The timing of gas reaching the surface and the averaged gas void fraction in the gas kick section show a satisfying match.

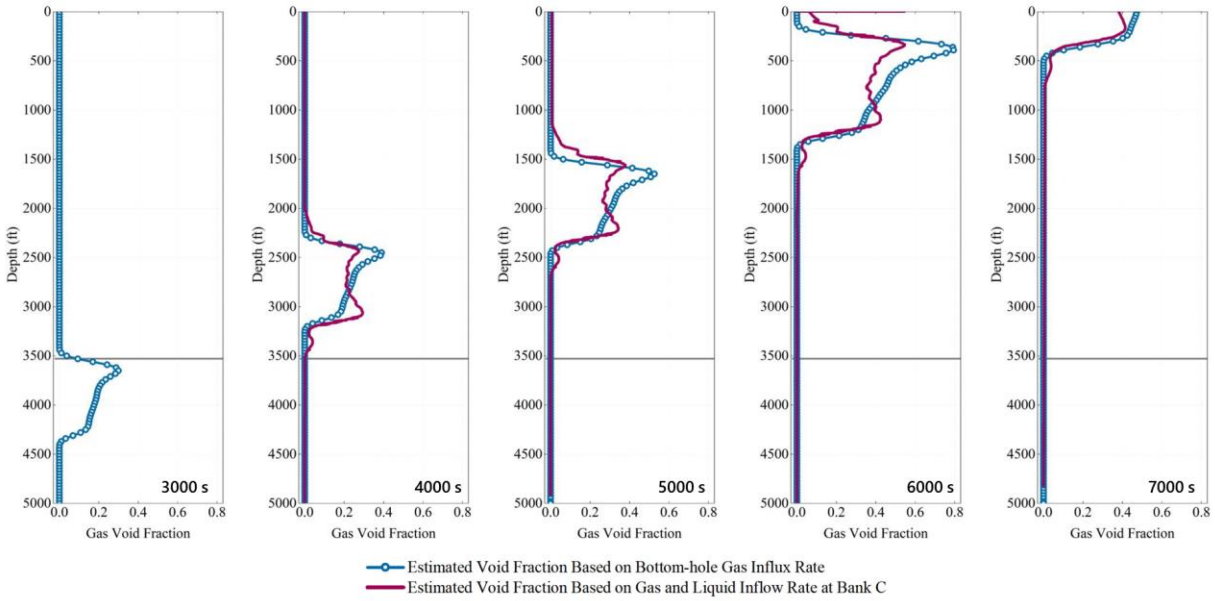

Fig. 12. Gas Void Fraction Profiles at Different Times During the Circulation of Gas Influx

3.4 Results Validation Based on Distributed Acoustic Sensing (DAS) Data

To further validate the accuracy of the estimated void fraction profiles over time, the measured data from Distributed Acoustic Sensing are compared with the calculation results. In **Fig. 14**, the void fraction profile of each timestep is plotted in a heat map, where the color represents the value of the void fraction. In the mapping of DAS measurement, the range of color represents the acoustic energy directly measured using the fiber optic sensor.

In the experimental wellbore, the optical fiber-based Distributed Acoustic Sensors (DAS) were installed outside of the tubing string (simulated drill-pipe) and used to record the change of acoustic energy during the migration/circulation process of gas influx. Distributed optical fiber sensors map physical fields acting on the fiber by exploiting the scattering processes that take place within the fiber when probed with an optical signal. During real-time data recording, low-frequency (0-0.5 Hz) DAS data was generated using a moving average based on 10 s recording length and later resampled at 1 s interval from the raw data.

A strong positive low-frequency data corresponds to the fiber section experiencing dynamic tensile strain, while a strong negative low-frequency DAS data indicate that section of the fiber is likely undergoing compression. By analyzing the DAS data, it is possible to directly identify the upper or lower boundaries of the gas influx section in the wellbore and their moving trajectory over time (as shown in **Fig. 13**). This data is greatly beneficial for validating the estimation results of gas influx distribution and migration behaviors.

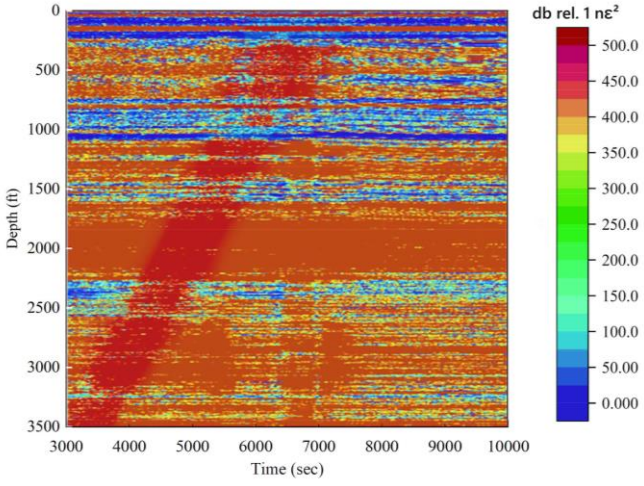

Fig. 13. Distributed Acoustic Sensing Measurements During The Full-Scale Experiment

Fig 13 demonstrates the processed DAS measurement data during the injection and gas circulation process. The warmer color represents higher acoustic energy, and according to **Fig 13**, a moving trace of the gas influx section can be identified.

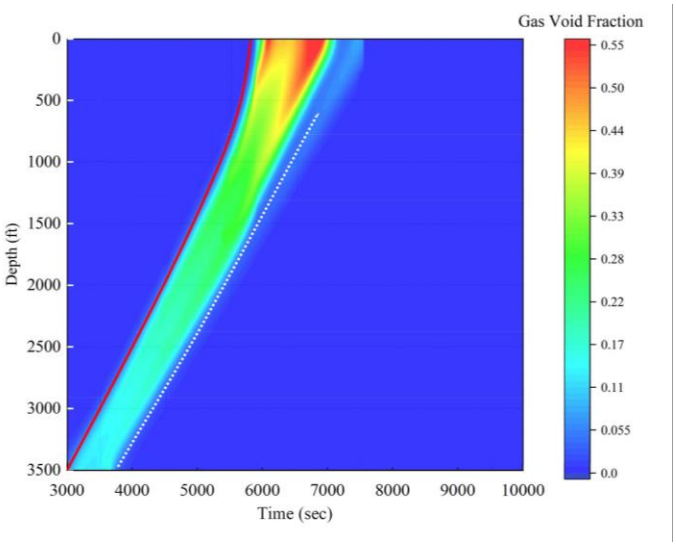

Fig. 14. Gas Void Fraction Heat Map Versus Time

Fig. 14 shows a heat map that represents the change of void fraction profiles over time during the gas injection and circulation process. The red and white dotted lines in Figure 20 represent the identified front and tail of the gas section from the distributed acoustic sensing data (**Fig. 13**). Good agreement can be observed between the estimation results and the DAS measurement. Based on the calculation results from the estimated gas influx rate using the data assimilation method, the observation of free gas reaching the surface is approximately 97 mins after the stop of injection. From the fiber-optic plotting, the actual observation of gas at the surface is at 95 mins after the end of gas injection. The above results proved the good performance of the Extended Kalman Filter in estimating the real-time gas influx rate and gas void fraction in the riser during riser gas events.

CONCLUSIONS

This study presented a data assimilation approach for the improved modeling and understanding of gas influx behaviors during riser gas events. The method proposed uses a Joint Extended Kalman Filter for estimating both liquid and gas inflow rates at the SSBOP level, as well as the tuning of model coefficients. Data from a full-scale experimental well is used in this study. The following conclusions were given based on a series of numerical simulations:

First, the Extended Kalman Filter performs well in handling input data and measurement data with random noises. The DFM implemented with the EKF shows higher estimation accuracy to the pressure at different depths compared to only the DFM without data assimilation methods. This study first used a multi-dimensional measurement for estimating the wellbore state in a gas kick scenario. Simulation results show that higher-dimensional measurements help to reduce the accumulative error along the wellbore.

Secondly, by analogizing the full-scale experimental wellbore into an offshore well that consists of a riser section and a lower wellbore section, riser gas events were replicated by the experiments and simulated by the proposed transient two-phase flow simulator. Using the bottom pressure, surface casing pressure, liquid outflow rate, and pump rate as input data, the inflow rate of both liquid and gas were accurately estimated at the depth of the SSBOP. The estimated gas void fraction profiles show a good agreement with a set of results that is directly based on accurate inflow rate measurements. And finally, the gas migration behavior and void fraction profiles show good agreement with the Distributed Acoustic Sensing (DAS) data.

This study presented an approach to enhance the accuracy of the physics-based models by using real-time measurement. The novelty of this work is seen by the application of EKFs in managing riser gas events and considering both liquid and gas inflow rate as unknown parameters, and applying reverse estimations of both using real-time measurements (instead of only having gas influx rate considered unknown for an onshore gas kick scenario). This study is beneficial for a better understanding of the gas influx behaviors inside a riser and the improved prediction accuracy for model-based decision makings with MPD.

Acknowledgment

This work is supported by the Louisiana Board of Regents (Grant contract number LEQSF (2019-22)-RD-B-02) and Louisiana State University Craft & Hawkins Department of Petroleum Engineering. The authors would also like to thank Oscar Gabaldon and Pedro Sousa from Blade Energy Partners for helpful suggestions and support.

Nomenclature

A	=	cross-sectional area open to flow [in^2]
A_D	=	single well drainage area [$acre$]
$a_{g,l,m}$	=	sonic velocity of gas, liquid, mixture [ft/s]
B_o	=	oil formation volume factor [bbl/STB]
C_0	=	distribution parameter in slip law
$C_{0d,1d}$	=	slip coeffects
C_f	=	friction coefficient
$D_{o,i}$	=	outer, inner diameter [in]
f	=	friction factor

g	=	acceleration of gravity [$\mathrm{m \cdot s^{-2}}$]
k_e	=	formation effective permeability [mD]
p	=	pressure [psi]
p_c	=	backpressure [psi]
Pr	=	Prandtl number
r_e	=	single well drainage radius [ft]
r_w	=	wellbore radius [ft]
$\boldsymbol{S}(w)$	=	vector of the source term
S_p	=	pressure source term [psi/ft]
t	=	time [s]
V_L	=	liquid volume [$\mathrm{m^3}$]
v_{gr}	=	drift velocity in slip law [ft/s]
$v_{g,l,m}$	=	gas, liquid, mixture velocity [ft/s]
$v_{sg,sl}$	=	superficial gas, liquid velocity [ft/s]
$\boldsymbol{w}$	=	vector of conservative variables
$w_{1,2,3}$	=	conservative variables

Greek Letters:

$\alpha_{g,l}$	=	volume fraction of gas, liquid [$\mathrm{lbm/s^2}$]
$\rho_{g,l,m}$	=	density of gas, liquid, mixture [ppg]
$\gamma_{g,l,m}$	=	relative density of gas, liquid, mixture
θ	=	wellbore inclination [°]
$\mu_{g,l,m}$	=	viscosity of gas, liquid, mixture [cp]

REFERENCES

Daireaux, B., Cayeux, E., Haavardstein, S., & Stokland, L. M. (2017, March). Use of Quantitative Risk Analysis Methods to Determine the Expected Drilling Parameter Operating Window Prior to Operation Start: Example From Two Wells in the North Sea. In SPE/IADC Drilling Conference and Exhibition. OnePetro.

Daireaux, B., Cayeux, E., Haavardstein, S., & Stokland, L. M. (2017, March). Use of Quantitative Risk Analysis Methods to Determine the Expected Drilling Parameter Operating Window Prior to Operation Start: Example From Two Wells in the North Sea. In SPE/IADC Drilling Conference and Exhibition. OnePetro.

Evje, Steinar, and Huanyao Wen. "Global solutions of a viscous gas-liquid model with unequal fluid velocities in a closed conduit." SIAM Journal on Mathematical Analysis 47.1 (2015): 381-406.

G.-O. Kaasa, Ø. N. Stamnes, O. M. Aamo, and L. S. Imsland, "Simplified hydraulics model used for intelligent estimation of downhole pressure for a managed-pressure-drilling control system," SPE Drilling and Completion, vol. 27, no. 1, pp. 127–138, March 2012.

Gavrilyuk, S. L., and J. Fabre. "Lagrangian coordinates for a drift-flux model of a gas-liquid mixture." International journal of multiphase flow 22.3 (1996): 453-460.

Gravdal, J. E., Lorentzen, R. J., & Time, R. W. (2010, October). Wired drill pipe telemetry enables real-time evaluation of kick during managed pressure drilling. In SPE Asia pacific oil and gas conference and exhibition. OnePetro.

Gu, Q., Fallah, A., Ambrus, A., Ma, Z., Chen, D., Ashok, P., & van Oort, E. (2020). A Switching MPD Controller for Mitigating Riser Gas Unloading Events in Offshore Drilling. SPE Drilling & Completion.

H. P. Lohne, J. E. Gravdal, E. W. Dvergsnes, G. Nygaard, and E. H. Vefring, "Automatic calibration of real-time computer models in intelligent drilling control systems - results from a north sea field trial," in International Petroleum Technology Conference, no. 12707- MS. Kuala Lumpur, Malaysia: International Petroleum Technology Conference, December 2008.

H. P. Lohne, J. E. Gravdal, E. W. Dvergsnes, G. Nygaard, and E. H. Vefring, "Automatic calibration of real-time computer models in intelligent drilling control systems - results from a north sea field trial," in International Petroleum Technology Conference, no. 12707- MS. Kuala Lumpur, Malaysia: International Petroleum Technology Conference, December 2008.

J. E. Gravdal, R. J. Lorentzen, K. K. Fjelde, and E. H. Vefring, "Tuning of computer model parameters in managed-pressure drilling applications using an unscented-Kalman-filter technique," SPE Journal, vol. 15, no. 3, pp. 856–866, 2010.

Jiang, Hailong, et al. "Numerical Simulation of a New Early Gas Kick Detection Method Using UKF Estimation and GLRT." Journal of Petroleum Science and Engineering, vol. 173, no. July 2018, Elsevier B.V., 2019, pp. 415–25, doi:10.1016/j.petrol.2018.09.065.

Julier, S. J., & Uhlmann, J. K. (1997, June). A non-divergent estimation algorithm in the presence of unknown correlations. In Proceedings of the 1997 American Control Conference (Cat. No. 97CH36041) (Vol. 4, pp. 2369-2373). IEEE.

Julier, Simon J., and Jeffrey K. Uhlmann. "New extension of the Kalman filter to nonlinear systems." Signal processing, sensor fusion, and target recognition VI. Vol. 3068. International Society for Optics and Photonics, 1997.

Kaasa, G. O., Stamnes, Ø. N., Imsland, L., & Aamo, O. M. (2012). Simplified hydraulics model used for intelligent estimation of downhole pressure for a managed-pressure-drilling control system. SPE Drilling & Completion, 27(01), 127-138.

Lohne, H. P., Gravdal, J. E., Dvergsnes, E. W., Nygaard, G., & Vefring, E. H. (2008, December). Automatic calibration of real-time computer models in intelligent drilling control systems-results from a north sea field trial. In IPTC 2008: International Petroleum Technology Conference (pp. cp-148). European Association of Geoscientists & Engineers.

Lorentzen, R. J., et al. "Tuning of Parameters in a Two-Phase Flow Model Using an Ensemble Kalman Filter." International Journal of Multiphase Flow, vol. 29, no. 8, 2003, pp. 1283–309, doi:10.1016/S0301-9322(03)00088-0.

Nikoofard, Amirhossein, et al. "Estimation of States and Parameters of a Drift-Flux Model with Unscented Kalman Filter." IFAC-PapersOnLine, vol. 28, no. 6, Elsevier Ltd., 2015, pp. 165–70, doi:10.1016/j.ifacol.2015.08.026.

Nikoofard, Amirhossein, et al. "Evaluation of Lyapunov-Based Adaptive Observer Using Low-Order Lumped Model for Estimation of Production Index in Under-Balanced Drilling." IFAC-PapersOnLine, vol. 28, no. 8, Elsevier Ltd., 2015, pp. 69–75, doi:10.1016/j.ifacol.2015.08.159.

O'brien, T. P., Lorentzen, K. R., Mann, I. R., Meredith, N. P., Blake, J. B., Fennell, J. F., ... & Anderson, R. R. (2003). Energization of relativistic electrons in the presence of ULF power and MeV microbursts: Evidence for dual ULF and VLF acceleration. Journal of Geophysical Research: Space Physics, 108(A8).

R. Lorentzen, G. Nævdal, and A. Lage, "Tuning of parameters in a two-phase flow model using an ensemble Kalman filter," International Journal of Multiphase Flow, vol. 29, no. 8, pp. 1283–1309, August 2003.

Romo, L., & Plaisance, M. (2015). IADC Deepwater Well Control Guidelines.

Sabah, M., Talebkeikhah, M., Agin, F., Talebkeikhah, F., & Hasheminasab, E. (2019). Application of decision tree, artificial neural networks, and adaptive neuro-fuzzy inference system on predicting lost circulation: A case study from Marun oil field. Journal of Petroleum Science and Engineering, 177, 236-249.

Schubert, J. J., Juvkam-Wold, H. C., & Choe, J. (2006). Well control procedures for dual gradient drilling as compared to conventional riser drilling. SPE Drilling & Completion, 21(04), 287-295.

Science, Applied. Real Time Kick Estimation and Monitoring in Managed Pressure Drilling System by © M . Musab Habib School of Graduate Studies in Partial Fulfillment of the Requirement for the Degree of Master of Engineering Faculty of Engineering and Applied Science Memor. no. May, 2020.

Swanson, B. W., Gardner, A. G., Brown, N. P., & Murray, P. J. (1997). Slimhole early kick detection by real-time drilling analysis. SPE Drilling & Completion, 12(01), 27-32.

Van Der Merwe, R., & Wan, E. (2003, April). Gaussian mixture sigma-point particle filters for sequential probabilistic inference in dynamic state-space models. In 2003 IEEE International Conference on Acoustics, Speech, and Signal Processing, 2003. Proceedings.(ICASSP'03). (Vol. 6, pp. VI-701). IEEE.

Van Der Merwe, R., & Wan, E. A. (2001, May). The square-root unscented Kalman filter for state and parameter-estimation. In 2001 IEEE international conference on acoustics, speech, and signal processing. Proceedings (Cat. No. 01CH37221) (Vol. 6, pp. 3461-3464). IEEE.

Van Der Merwe, Rudolph, and Eric A. Wan. "The square-root unscented Kalman filter for state and parameter-estimation." 2001 IEEE international conference on acoustics, speech, and signal processing. Proceedings (Cat. No. 01CH37221). Vol. 6. IEEE, 2001.

Wang Z.Y., Sun BJ Deepwater gas kick simulation with consideration of the gas hydrate phase transition[J]. Journal of Hydrodynamics, Ser. B, 2014, 26(1):94–103.

Wei, C., & Chen, Y. (2021). On Improving Algorithm Efficiency of Gas-Kick Simulations toward Automated Influx Management: A Robertson Differential-Algebraic-Equation Problem Approach. SPE Drilling & Completion, 36(04), 943-966.

Wei, L., Yang, X., Xi, C., Hong, C., Yumin, L., & Xueqing, L. (2020). Research and application of downhole blowout prevention system while drilling: A review. Journal of Petroleum Science and Engineering, 188, 106882.

Wielitzka, Mark, et al. "Joint Unscented Kalman Filter for State and Parameter Estimation in Vehicle Dynamics." 2015 IEEE Conference on Control and Applications, CCA 2015 - Proceedings, no. 978, EUCA, 2015, pp. 1945–50, doi:10.1109/CCA.2015.7320894.

Zuber, Novak, and JAa Findlay. "Average volumetric concentration in two-phase flow systems." (1965): 453-468.